

SUPPLEMENTARY INFORMATION

Tailoring defects and nanocrystal transformation for optimal heating power in bimagnetic $\text{Co}_y\text{Fe}_{1-y}\text{O}@Co_x\text{Fe}_{3-x}\text{O}_4$ particles

George Antonaropoulos,^{a,b} Marianna Vasilakaki,^c Kalliopi N. Trohidou,^c Vincenzo Iannotti,^d Giovanni Ausanio,^d Milinda Abeykoon^e, Emil S. Bozin^f and Alexandros Lappas^{*a}

- a. *Institute of Electronic Structure and Laser, Foundation for Research and Technology - Hellas, Vassilika Vouton, 71110 Heraklion, Greece*
- b. *Department of Chemistry, University of Crete, Voutes, 71003 Heraklion, Greece*
- c. *Institute of Nanoscience and Nanotechnology, National Center for Scientific Research Demokritos, 15310 Athens, Greece*
- d. *CNR-SPIN and Department of Physics "E. Pancini", University of Naples Federico II, Piazzale V. Tecchio 80, 80125 Naples, Italy*
- e. *Photon Sciences Division, National Synchrotron Light Source II, Brookhaven National Laboratory, Upton, New York 11973, USA*
- f. *Condensed Matter Physics and Materials Science Division, Brookhaven National Laboratory, Upton, New York 11973, USA*

*Corresponding author: lappas@iesl.forth.gr

Table of Contents

S1. Monte Carlo calculation of H_{EB} and H_C	3
Figure S 1. MC simulation results for exchange bias, H_{EB} and coercive field, H_C	3
Figure S 2. MC simulation results for exchange bias, H_{EB} and coercive field, H_C	4
S2. Calculation of the Specific Absorption Rate (SAR).....	5
Table S 1. Number and type of spins in each nanoparticle region, used for Monte Carlo calculations.....	6
Figure S 3. Cubic Sample C7 (7% Co).....	7
Figure S 4. SEM-EDS spectra	8
Figure S 5. xPDF fits of data for bulk reference $CoFe_2O_4$	9
Figure S 6. xPDF fits of NP data	10
Figure S 7. Co(%) -dependence of the blocking temperature (T_B)	11
Table S 2. Crystallographic parameters of the cubic spinel model and cubic rock salt model.....	12
Table S 3. Parameters for the nanocrystal samples.....	13
Figure S 8. The experimentally determined M_r/M_s	14
Figure S 9. The low-field, normalized hysteresis loop regions at 5 K	15
Table S 4. Morphological and magnetic characteristics of nanocrystal samples	16
References	17

S1. Monte Carlo calculation of H_{EB} and H_C

In order to give a deeper insight on the effect of Co substitution in combination with the defects in Model #1, where the core/shell ratio is 25%/75% and the defects are located only in the core, we considered nanoparticles described by variants of Model #1: a) without defects (def=0%), b) without Co (substitution = 0%), c) without defects and Co (def=0% and substitution = 0%) and we compare these results with the starting model (Co=10% and def=40% in the core and core IF). Figure S1 presents the MC results of the H_{EB} and the H_C as a function of the cooling field.

In the case of the model variant, where Co is absent (blue line), the bonds at the interface become more ordered than those of starting Model #1 (black line) and this enhances the competition between the soft and the hard component at the core/shell (AFM/FiM) interface, increasing the exchange bias field. In the model variant where Co exists, but no defects are present (red line), the soft component along the interface is marginally enhanced, resulting to a small increase of H_{EB} . Finally, when both substitution and defects are absent (green line), we observe an imperceptible decrease of the H_{EB} . In all cases the absence of pinning centers either in the core (Co and defects) or the shell (Co sites) makes the H_C noticeably diminishing. Thus, it seems that the enhancement of the H_{EB} and H_C values can be achieved with a relatively small, defected AFM core in a combination with a low Co percentage. Taking into account the calculated values for a similarly-sized, non-substituted core@shell particle ("pure" in Fig. 11b, main text), it seems that given an ideal core@shell particle with no defects at all in the shell, any combination of defects and Co% in the core would result to a similar total magnetic response, if not higher. The only way to noticeably lower the H_C value, is to create a perfectly ordered FeO core, with no defects and Co sites (green line). This is though impossible to be achieved experimentally, due to the highly sub-stoichiometric nature of $Fe_{1-x}O$. Therefore, we conclude that substituting a particle's core only, is not followed by severe changes in the total magnetic response, apart from the stabilization of the core (protection against oxidation), which is obviously a key element for the emergence of exchange interactions at the interface. Since chemical substitution in our synthetic protocol is leading to Co incorporation in the shell as well, a similar analysis to investigate the combined actions of Co-substitution and defects in the shell only, has been done.

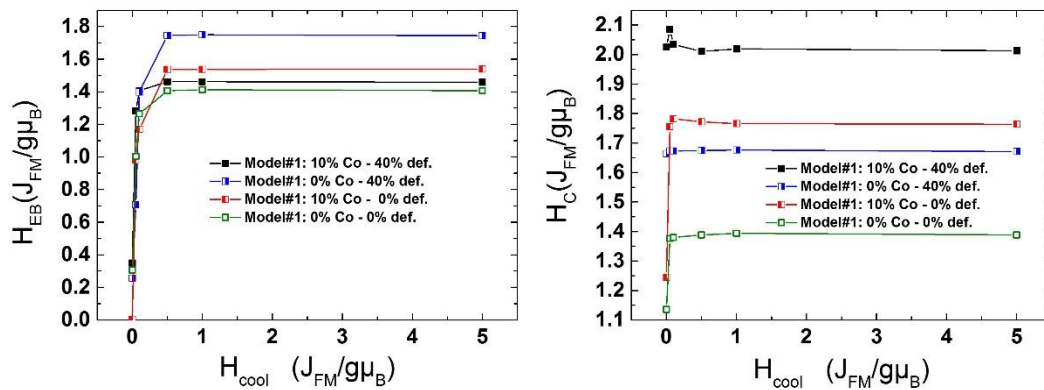


Figure S1. MC simulation results for exchange bias, H_{EB} and coercive field, H_C for different simulated cooling fields, H_{cool} for variations in composition of model #1, as detailed in the graph legends. While keeping the morphological characteristics of the simulated nanoparticles the same, we tested different combinations of Co substitution and defects (vacant crystallographic sites). The lines connecting the points, extracted from the calculations, are a guide to the eye.

This was performed by simulating different variants of model #2, in which the core/shell ratio is 50%/50% and the defects are located in the shell only. MC simulated results for the cooling field dependence of the H_{EB} and H_C are shown in Figure S2 for the cases of model #2 a) without defects (red line), b) without Co (blue line), c) without Co and defects (green line) and d) an additional variant of reduced population of defects (orange line). The results are again compared with those for the starting model (Co=35% and def=40% in the shell) shown with the black line. Interestingly, when comparing the 2 Co-substituted nanoparticle model variants with defects (black and yellow line) and the one without defects in its structure (red line), as the population of defects becomes smaller and smaller and finally drops to zero, the fraction of defects at the shell IF also diminishes, resulting in a stronger shell-IF magnetization component. Thus the competition with the core-IF is raising and the exchange bias gradually increases too. This does not affect the H_C which remains almost the same, due to the contribution of the large fractions of Co sites in the magnetocrystalline anisotropy. When Co and defected sites are absent (green line) in an ideal perfectly ordered spinel ferrite, this seems to negatively affect the effective shell interface anisotropy and further weakens the competition between the two phases at the interface, decreasing the H_{EB} , but not considerably. A high rate of defects (40%), without any Co sites (blue line), worsens the situation even more, since the shell-IF magnetization component seems unable to maintain a proper magnetic ordering to oppose the AFM core. The depletion of the magnetocrystalline anisotropy when the Co sites are absent, also decreases the H_C (blue and green line in Figure S2, right panel). Overall, the optimum magnetic behaviour in this case (core/shell = 50%/50%) can be achieved with a non-defective and highly Co substituted FiM shell. The H_{EB} values are in the case of model #2 significantly lower than those in model #1 and the pure, non-substituted model due to the lower volume fraction of FiM shell, giving the AFM core the opportunity to prevail.

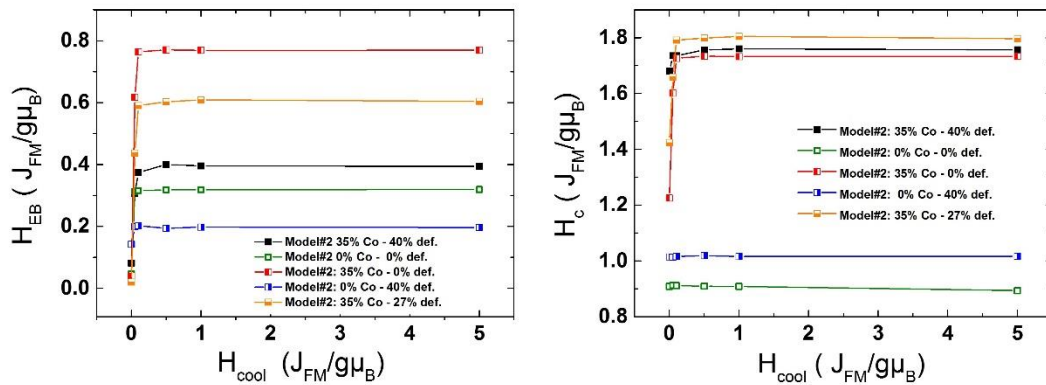


Figure S 2. MC simulation results for exchange bias, H_{EB} and coercive field, H_C , for different simulated cooling fields, H_{cool} for variations of composition in model #2, as detailed in the graph legends. We keep again the morphological characteristics of the simulated nanoparticles the same and test different combinations of Co-levels and defects (vacant crystallographic sites). The lines connecting the points, extracted from the calculations, are a guide to the eye.

S2. Calculation of the Specific Absorption Rate (SAR)

The above calculations of H_c and H_{EB} as a function of the cooling field were performed for low temperature (as in the experiments). For the following calculations, the Néel-Brown relaxation model^{1,2} is used to calculate the SAR due to susceptibility losses. Therefore, for our calculations the experimental values at $T=313$ K have been used.

The Specific Absorption Rate is expressed as:
$$SAR(f) = \frac{\mu_0 \pi f \chi'' H_0^2}{\rho}$$

where ρ : average density of each ferrite nanoparticle equals to $V_{core}/V_{tot} \times \rho_{Fe_{1-y}Co_yO} + V_{shell}/V_{tot} \times \rho_{Fe_{3-y}Co_yO_4}$ and $\rho_{Fe_{1-y}Co_yO} = 8 \times M_W / 0.602 \times \alpha^3_{Fe_{1-y}Co_yO}$ and $\rho_{Fe_{3-y}Co_yO_4} = 4 \times M_W / 0.602 \times \alpha^3_{Fe_{3-y}Co_yO_4}$ with M_W : molecular weight and α : lattice constant

H_0 : AC field amplitude, and f : field frequency,

χ'' : imaginary part of the complex susceptibility that involves the effective relaxation times for the two absorption mechanisms, namely, Brown (τ_B) and Néel (τ_N).

Temperature is set to $T=313$ K.

η : the medium viscosity with a value of 0.65×10^{-3} Pa.s (approximately the value for water at 40°C)

ϕ : volumetric ratio of the NPs set to 0.001

A surfactant layer that covers the nanoparticles (NPs) is taken to have a thickness of 4 nm that is a parameter introduced in the calculation for the Brownian relaxation time.³

In our calculations the effective nanoparticle anisotropy constant is taken from the equation: $(KV)_{eff} = 25k_B T_B$ where T_B is the blocking temperature extracted from the experimental ZFC magnetization curves and V the volume of the particles. The saturation magnetization M_S at 300K is extracted from the experimental hysteresis loops of the Co-substituted nanoparticles. For comparison purposes, we considered also the experimental values for the defected spherical nanoparticles named S15 and the S8 magnetite NPs of $D=15$ and 8 nm respectively.³

Exploring the effect of AC field strength, the SAR according to the Linear Response Theory for the Néel-Brown relaxation model,¹ was calculated at different field amplitudes, H_0 , with a frequency of $f=500$ kHz. The difference in the magnitude of SAR (due to susceptibility losses) of Co substituted and defected compared to pure and defected NPs is depicted in the plot shown in Fig. 12. The SAR (H_0) curves follow a trend similar to that in experimental findings previously reported.⁴ The higher anisotropy volume of the core/shell nanoparticles results in the deviation from the quadratic field dependence of the SAR curve, which the smaller particle S8 only follows.⁵

Table S 1. Number and type of spins in each nanoparticle region, used for Monte Carlo calculations for the three heterostructured nanocrystal models, illustrated in Fig. 1 (main text). The corresponding relative volume fractions and Co percentages are also noted for quick reference.

		Total	Pure sites	Defects	Doped site	% Volume	% Doping
pure	Core	257	196	61	0	20	0
	Core-IF	330	319	11	0		
	Shell-IF	362	351	11	0	80	
	Shell	2170	1475	695	0		
model #1	Core	461	170	284	7	25	10
	Core-IF	338	224	36	78		
	Shell-IF	558	498	0	60	75	
	Shell	1762	1585	0	177		
model #2	Core	1021	658	0	363	50	35
	Core-IF	530	349	0	181		
	Shell-IF	654	261	55	338	50	
	Shell	914	124	577	213		

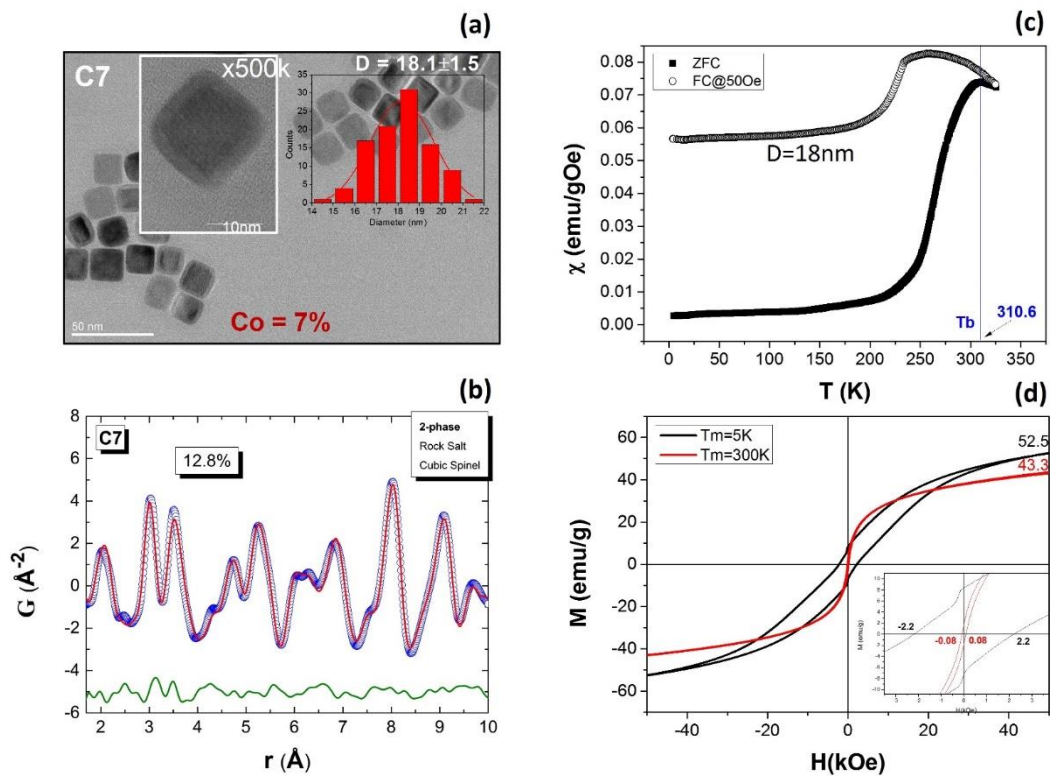


Figure S3. Cubic Sample C7 (7% Co): (a) Low-magnification bright field TEM images of a cubic sample, entailing an edge length of ~ 18 nm and inset of HR-TEM showing a clear core@shell structure. (b) xPDF fit of data at $T = 300$ K over the low- r PDF region (1 nm) for the same sample, assuming a 2-phase rock-salt/cubic spinel model ($Fm\text{-}3m/Fd\text{-}3m$, $R_w = 12.8\%$). (c) Temperature evolution of the zero-field cooled (ZFC, solid line) and field-cooled (FC, dotted line) susceptibility curves, under a magnetic field of 50 Oe. (d) The low-field part of the hysteresis loop at 5 K and 300 K, taken under zero- and field-cooled ($H_{cool} = 50$ kOe) protocols.

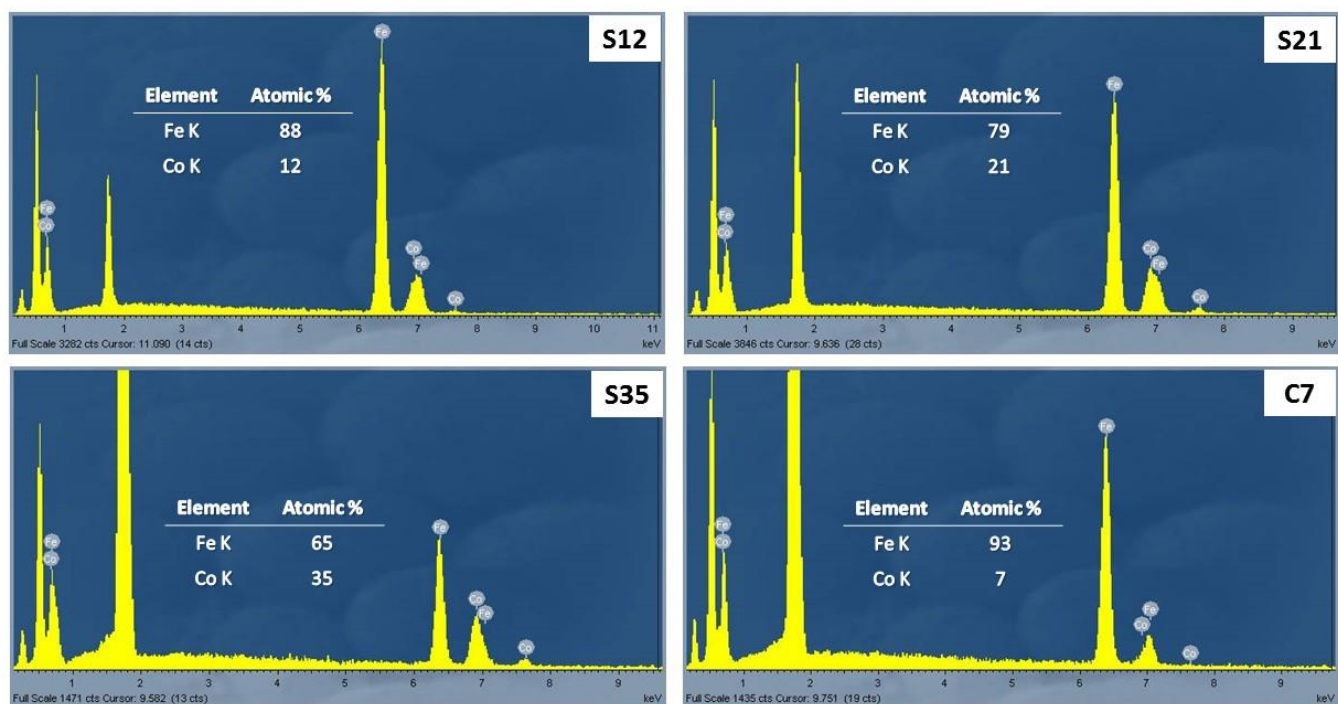


Figure S 4. SEM-EDS spectra showing the characteristic K-peaks of Fe and Co of the three studied spherical nanocrystal samples (S12, S21, S35) and one cubic (C7). Their relative atomic % abundance is automatically calculated by INCA software. The peak at ~1.8 keV is coming from the Si substrate and this is why it is in some case too high compared to Fe and Co peaks.

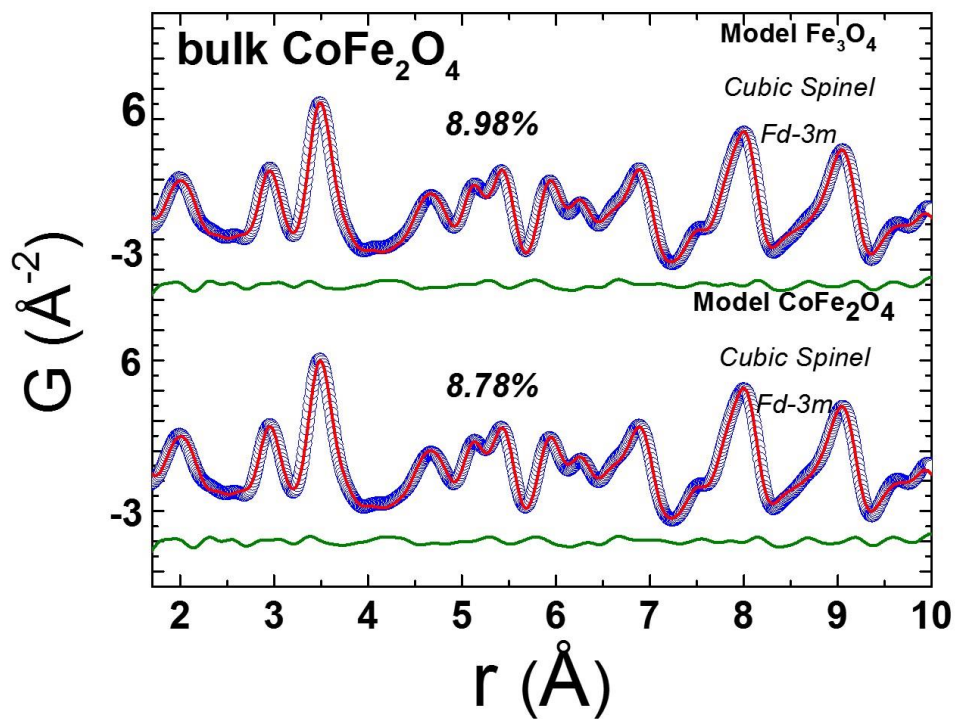


Figure S 5. xPDF fits of data at $T= 300$ K over the low- r PDF region (1 nm) for bulk reference CoFe_2O_4 assuming a Fe_3O_4 , cubic spinel model (Fd-3m, $R_w= 8.98\%$) at the top and a CoFe_2O_4 cubic spinel model (Fd-3m, $R_w= 8.78\%$) at the bottom, where half of the Fe-ions in the octahedral sites of the model shown at the top, have been replaced by Co, resembling the simplest cobalt ferrite cubic spinel structure. These two models are practically equally good in describing the structure, since xPDF cannot distinguish between Fe and Co ions.

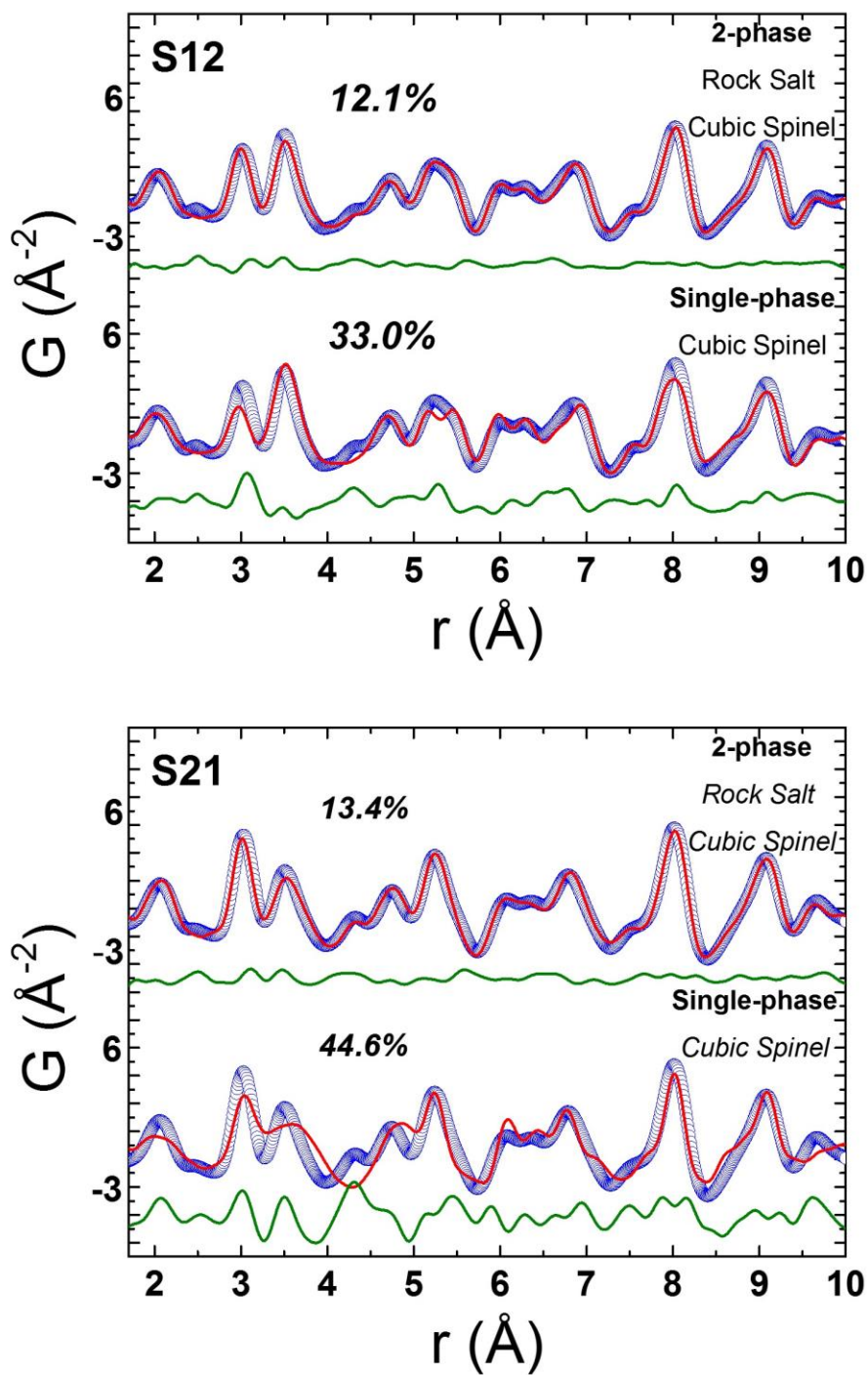


Figure S 6. xPDF fits of data at $T = 300$ K over the low- r PDF region (1 nm) for sample S12 (top, $R_w = 33.0\%$ vs. 12.1%) and S21 (bottom, $R_w = 44.6\%$ vs. 13.4%), assuming either a single-phase, spinel-only model or a 2-phase rock-salt/cubic spinel model (Fm-3m/ Fd-3m).

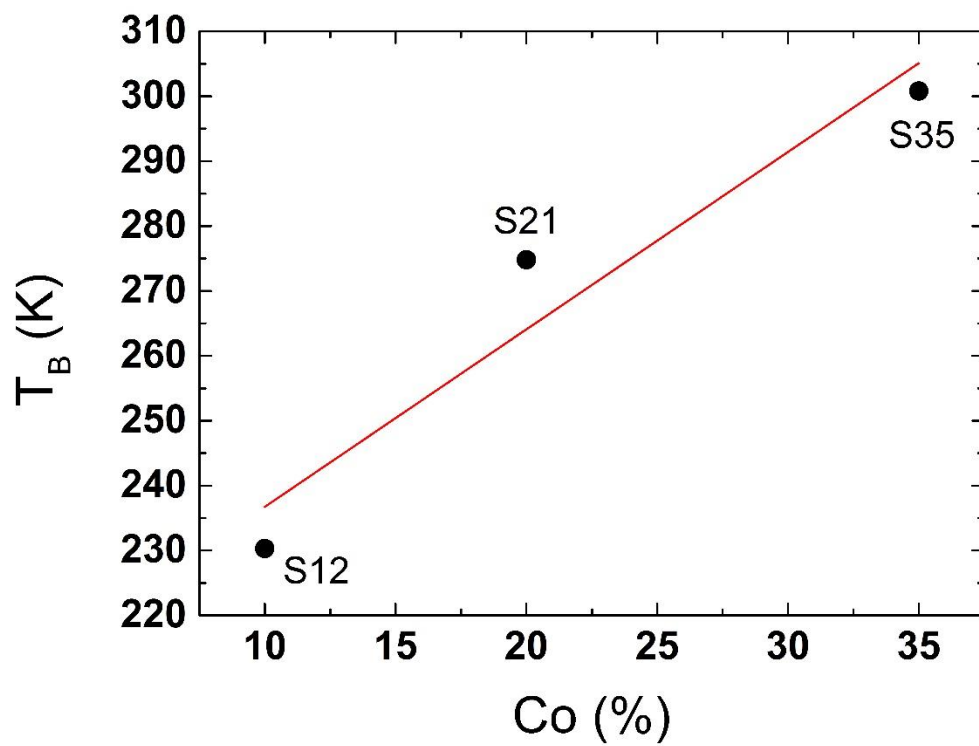


Figure S 7. Dependence of the blocking temperature (T_B) as extracted from the maximum of the zero-field cooled (ZFC) magnetic susceptibility curves (Fig. 9 – main text) for the spherical nanocrystal samples S12, S21 and S35, showing a nearly linear increase of T_B , as Co-content increases.

Table S 2. Crystallographic parameters of the cubic spinel and rock salt models utilized in the refinements of the low-r atomic PDF ($r=1-10 \text{ \AA}$) and parameters for bulk reference samples derived from fitting the low-r region of their atomic PDF.

	refined parameters			
	Models		Reference Samples	
	Spinel ^[*]	Rock Salt ^[**]	Bulk CoFe_2O_4	Bulk FeO
Symmetry	Fd-3m	Fm-3m	Fd-3m	Fm-3m
a (Å)				
b (Å)	8.397	4.3108	8.37699(4)	4.32151(5)
c (Å)				
V (Å³)	592.0692	80.1076	587.8466(1)	80.7061(1)
Fe-Td				
8α		0.003		
x=y=z	0.125	Uiso (Å ²)	0.125	Uiso (Å ²)
Uiso (Å²)	0.003		0.0068(1)	0.0120(5)
Fe-Oh				
16d		0		
x=y=z	0.5	x = y = z		0
Uiso (Å²)	0.003		0.0074(1)	x = y = z
O				
32e	0.2551	0.5	0.5	0.5
x=y=z				
Uiso (Å²)	0.003	0.003	0.0074(1)	0.0229(6)
% vol. fraction	100	100
Rw (%)	9.0	14.4

* see ref⁶

** see ref⁷

Table S3. Parameters for the nanocrystal samples, derived from fitting the low-r region of their atomic PDF ($r= 1-10 \text{ \AA}$) and σ_0 values extracted from the Einstein fit of their T-dependent isotropic temperature factors, giving the static disorder of the system.

refined parameters						
	S12		S21		S35	
	Spinel	Rock salt	Spinel	Rock salt	Spinel	Rock salt
Symmetry	Fd-3m	Fm-3m	Fd-3m	Fm-3m	Fd-3m	Fm-3m
a (Å)						
b (Å)	8.415(1)	4.305(1)	8.407(5)	4.296(2)	8.411(6)	4.295(1)
c (Å)						
V (Å³)	595.885(1)	79.785(1)	594.187(1)	79.285(1)	595.035(1)	79.230(1)
Fe-Td						
8α		0.0096(1)		0.0098(1)		0.0087(1)
x=y=z	0.125		0.125		0.125	
Uiso (Å²)	0.0088(1)	Uiso (Å ²)	0.0151(6)	Uiso (Å ²)	0.019(1)	Uiso (Å ²)
Fe-Oh						
16d		0		0		0
x=y=z	0.5	x = y = z	0.5	x = y = z	0.5	x = y = z
Uiso (Å²)	0.0086(1)	x = y = z	0.0118(4)	x = y = z	0.0101(5)	x = y = z
O						
32e		x=y=z 0.5		x=y=z 0.5		x=y=z 0.5
x=y=z	0.2551		0.2551		0.2551	
Uiso (Å²)	0.018(1)	Uiso (Å ²) 0.0288(3)	0.017(1)	Uiso (Å ²) 0.0254(2)	0.021(2)	Uiso (Å ²) 0.0231(2)
% vol. fraction	73.6(1)	26.4(1)	63.6(1)	36.4(1)	47.1(1)	52.9(1)
Rw (%)	12.1		13.4		10.2	
Oh σ₀	0.00343(2)	...	0.00419(1)	...	0.00312(2)	...
Td σ₀	0.00387(3)	...	0.00832(3)	...	0.00956(3)	...
RS σ₀	...	0.00377(2)	...	0.00324(2)	...	0.00242(2)

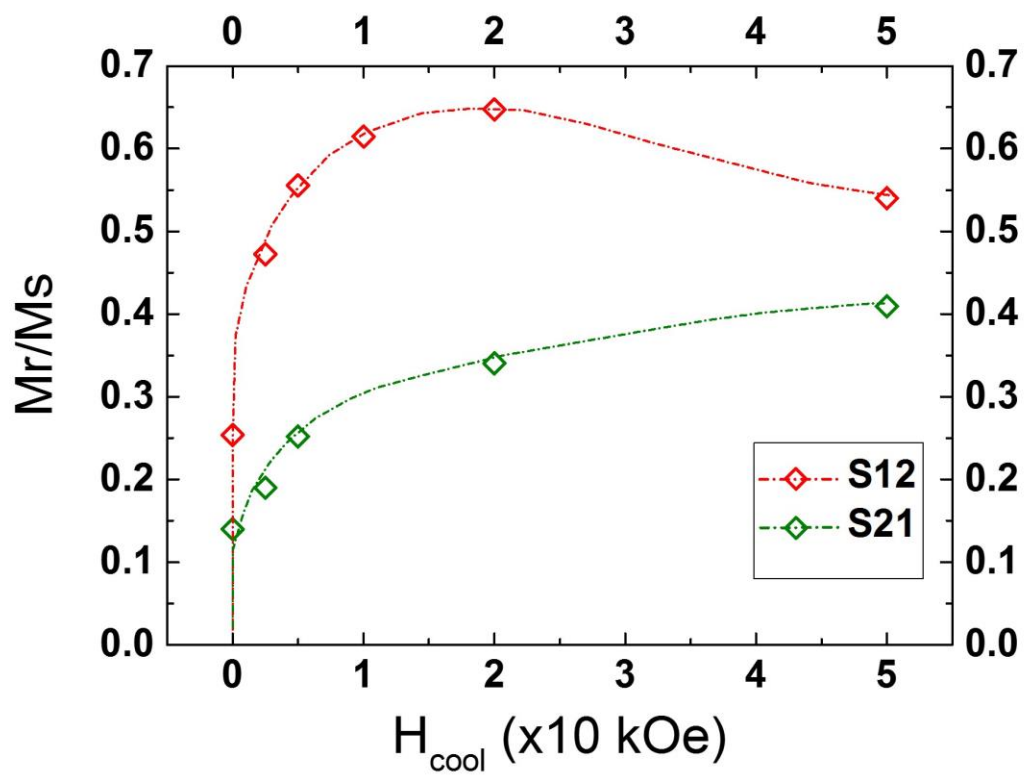


Figure S 8. The experimentally determined M_r/M_s ratio obtained at varying cooling-field strengths (H_{cool}) for nanocrystal samples S12 (red symbols) and S21 (green symbols). The lines are a guide to the eye.

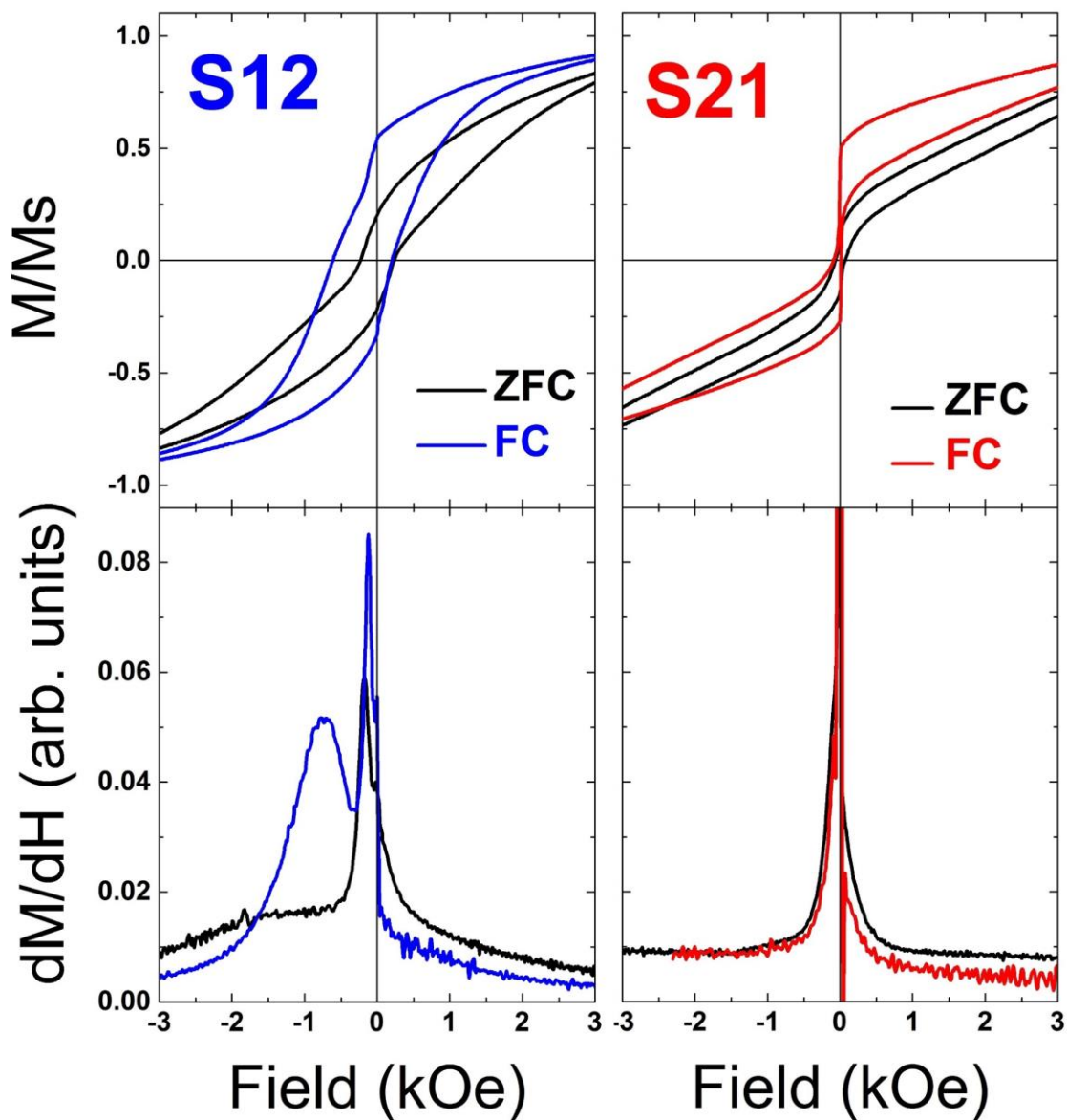


Figure S 9. The low-field, normalized hysteresis loop regions at 5 K, for samples S12 and S21, comparing the M/M_s data measured after 50 kOe field-cooled (FC, colored curves) and zero-field cooled (ZFC, black curves) protocols. The panels beneath the normalized magnetization M/M_s present the corresponding differential change (dM/dH) when switching from positive to negative field saturation.

Table S 4. Size and composition of nanocrystal samples, their blocking temperature T_B , as well as the saturation magnetization, M_S and the coercive field, H_c at $T= 5$ and 300 K. The field-cooled (FC) hysteresis loop (M - H ; $H_{cool} = 50$ kOe) characteristics, including exchange bias H_{EB} at 5 K for samples S12 and S21.

Sample	Size (nm)	Co%	T_B (K)	M_S (emu/g), 300K	H_c (Oe), 300K	M_S (emu/g), 5K	H_c (Oe), 5K	M_S (emu/g), FC curve, 5K	H_c (Oe), FC curve, 5K	H_{EB} (Oe)
S12	15.2	12	230	42.5	180	39.2	2350	50.7	2617	2022
S21	13.9	21	275	22.2	265	17	702	19.7	823	367
S35	17.8	35	301	14.8	335	12.4	1182	/	/	/
C7	18.1	7	311	43.3	87	52.5	2188	/	/	/

References

- 1 R. E. Rosensweig, *J. Magn. Magn. Mater.*, 2002, **252**, 370–374.
- 2 M. Vasilakaki, C. Binns and K. N. Trohidou, *Nanoscale*, 2015, **7**, 7753–7762.
- 3 A. Lappas, G. Antonaropoulos, K. Brintakis, M. Vasilakaki, K. N. Trohidou, V. Iannotti, G. Ausanio, A. Kostopoulou, M. Abeykoon, I. K. Robinson and E. S. Bozin, *Phys. Rev. X*, 2019, **9**, 041044.
- 4 G. Vallejo-Fernandez, O. Whear, A. G. Roca, S. Hussain, J. Timmis, V. Patel and K. O’Grady, *J. Phys. Appl. Phys.*, 2013, **46**, 312001.
- 5 T. E. Torres, E. Lima, M. P. Calatayud, B. Sanz, A. Ibarra, R. Fernández-Pacheco, A. Mayoral, C. Marquina, M. R. Ibarra and G. F. Goya, *Sci. Rep.*, 2019, **9**, 3992.
- 6 H. S. C. O’Neill and W. A. Dollase, *Phys. Chem. Miner.*, 1994, **20**, 541–555.
- 7 R. W. G. Wyckoff, in *Crystal Structures - Volume 1.*, Interscience Publishers, New York, 1963, pp. 85–237.